Modeling of a Rotaxane-Based Molecular Device

Xiange Zheng and Karl Sohlberg*

Department of Chemistry, Drexel University, 3201 Chestnut Street, Philadelphia, Pennsylvania 19104

Received: August 14, 2002; In Final Form: September 30, 2002

A computational procedure is presented for investigating photoinduced switchable rotaxanes and demonstrated for a known system. This procedure starts with the generation of $>10^4$ chemically reasonable rotaxane coconformations based on an empirical intramolecular potential-energy function. Each of the structures is then assigned by its gross structural features (coiled or extended) and by the position of the ring along the shaft. Single-point energy calculations at the semiempirical (AM1) level are then carried out for each structure in the singlet (ground), triplet, and anionic doublet states. The structural features are then correlated with energy for each state. What emerges is a profile of the structure−energy relationship that captures the salient features of the system that endow it with devicelike character. The full geometry optimization of a subset of the coconformations demonstrates that the procedure based on single-point calculations is sufficient to obtain a profile of the relationship of the structural features to energy that is consistent with experiments at a greatly reduced computational cost.

Introduction

The design, synthesis, and characterization of stimuli-responsive molecular devices and molecular machines present a great challenge.[1−6] The chemistry of macromolecular systems such as knots,[7] catenanes,[8] and especially rotaxanes has been of considerable interest in recent years[7−27] in part because they hold promise for the fabrication of prototype molecular devices. A rotaxane is an assembly of mechanically interlocked molecules in which a dumbbell-shaped component is encircled by one (or more) chemically independent cyclic component(s). For example, a rotaxane is created when a cyclodextrin ring (called the "shuttle" or "crown") is threaded with a linear chain (called the "shaft" or "chain") in which the shaft is terminated by a bulky substituent on each end to prevent the unthreading of the shuttle. The construction of molecular shuttles in which the ring shifts between two or more "stations" on the linear chain in response to external stimuli is one promising target for prototype molecular devices.[3,5,6,15,23,27−40] Numerous examples have been reported. Recently, Deetz et al. described the synthesis of four isomeric rotaxanes exhibiting coconformational exchange upon salt binding.[41] Kern and co-workers reported a molecular machinelike copper rotaxane observed by X-ray absorption spectroscopy experiments.[42] Glink and co-workers described temperature-controlled (−140 to +50 °C) molecular shuttles using rotaxanes.[38] Murakami et al. reported the results on a light-driven molecular shuttle based on manipulating a rotaxane's electromagnetic environment.[43] Martinez-Diaz et al. reported a pH-switchable rotaxane,[39] and Brouwer et al. described a photoinduced hydrogen-bond-assembled molecular shuttle.[44]

An impressive and steadily increasing range of prototype stimuli-responsive molecular devices has been reported. To facilitate the *systematic* design and refinement of functional molecular devices, it would be desirable to have available robust and validated modeling techniques. Such molecular device systems present a formidable challenge to computational chemistry, owing to the large size of the molecules involved. The simplest prototype rotaxane-based molecular devices involve nearly 200 atoms. Nevertheless, some pioneering modeling studies have been reported.[9,11,24,45−47] Asakawa et al.[9] described the transmission of chirality between rotaxane components using a combination of semiempirical calculations and geometrical modeling. Biscarini et al. reported the first molecular-mechanics-based, solid-state calculations on interlocked molecules to predict and test which rotaxanes are best suited as building blocks for crystalline-phase systems with mobile submolecular units.[11] Leigh et al. carried out the reduced-dimensionality quantum-mechanical modeling of macrocyclic ring rotation in benzylic amide catenanes[19] and rotaxane shuttling[48] and recovered rate constants in agreement with those obtained by temperature-dependent nuclear magnetic resonance measurements. They have applied similar reduced-dimensionality quantum-mechanical models to rotaxane shuttling.[48]

In this paper, it is our goal to demonstrate, *on an experimentally realized example*, a procedure for modeling rotaxane-based molecular devices that captures the features critical to their devicelike character. Specifically, we seek a modeling procedure that predicts the spontaneous shuttling of the ring relative to the shaft in a switchable rotaxane, herein for a system with redox-dependent bistability. Toward this end, an extensive investigation has been undertaken for one such photoinduced hydrogen-bonded rotaxane molecule. In this device,[44] the stoppers on the two ends of the chain component are succinamide (succ) and 3,6-di-*tert*-butyl-1,8-naphthalimide (ni) units, respectively, which are separated by a C_{12} alkyl spacer and serve as two potential H-bonding stations. The chain is encircled by a benzylic amide macrocyclic crown-ether ring molecule named 1,4,7,14,17,20-hexaaza-2,6,15,19-tetraoxo-3,5,9,12,16,18,22,25-tetrabenzocyclohexacosane that can be induced to change its position and shuttle between the succ and ni stations on the linear chain. The computational procedure includes conformational searching over the full torsional space of the rotaxane. This is followed by single-point semiempirical calculations for all coconformations in their neutral singlet, triplet, and anionic doublet states and statistical analysis to correlate the structural

* To whom correspondence should be addressed.

10.1021/jp0267611 CCC: $25.00
Published on Web 02/01/2003

features with energy in each state. The conformational searching was performed on the basis of all rotatable bonds of the two component molecules and generated $>10^4$ coconformations. The observed correlation was checked by repeating the analysis after full geometry optimizations on a subset of the coconformations (~1%). The overall procedure accurately captures the structural and switching characteristics of the physical system; therefore, the method shows promise to serve as a tool for molecular-device "design engineering".

Theoretical Methods

Computational Details. The initial rotaxane-structure generation was performed with a graphical-user-interface molecular editor.[49] The SCAN module in the Tinker molecular mechanics (MM) software[50−53] was employed for the conformational searching over all the full torsional space with the following modes and parameters: (1) automatically selecting torsional angles, (2) setting the number of searching directions for a local search at 50, (3) taking 50.0 kcal/mol as the energy threshold for the local minima, (4) setting the RMS gradient per atom criterion at 0.0001 kcal/(mol Å), and (5) setting the time limit for each search with a unique starting geometry at 1 h. The OPLS-AA[54−56] force-field parameter set was chosen, principally on the basis of the breadth of its parameterization. It is important to note that in this study MM methods served only for model building; that is, they were employed solely to identify an ensemble of reasonable geometric configurations of the rotaxane. The OPLS-AA force-field nonbonded- and torsional-energy parameters were originally derived to reproduce ab initio (RHF/6-31G*) structures[56] and should, therefore, lead to a suitable set of rotaxane configurations.

Semiempirical single-point calculations and geometry optimizations were performed with the AM1[57] method using the GAMESS program.[58] Previous success in treating inclusion phenomena with semiempirical methods[24,59,60] suggested that treating rotaxane systems semiempirically would be a judicious approximation. The semiempirical methods, like ab initio methods, are based on an inherently quantum-mechanical description of the electronic structure but are sufficiently efficient for practical calculations on systems of this size. The AM1 method has been found to be qualitatively acceptable for intermolecular hydrogen bonding,[61] the dominant interaction between host and guest here. Its performance is reported to be especially good if the comparisons are to be done within a class of compounds wherein the relative hydrogen-bond strengths are predicted with high accuracy.[61] Additional support for the choice of the AM1 method to identify the conformational preferences in the present rotaxane system comes from ref 62, wherein the AM1 calculations are reported for >60 conjugated organic molecules, many with structural subunits similar to those of the present rotaxane. It was found that, within the chosen set of compounds, the conformational preferences were "quite satisfactorily calculated". This assertion is reinforced by very recent work by Dávila and Caldas.[63] Finally, we note that the devicelike character of the system is embodied in its gross structural features, which should be captured accurately even at the semiempirical level of theory. Within the space of their parameterization, the empirical force-field (MM) techniques often actually outperform semiempirical quantum mechanics such as the AM1 or even not fully converged first-principles calculations.[64] A formally quantum-electronic-structure method is employed here for access to multiple electronic states without reparameterization. For computational expediency, solvent effects were neglected in this work. This approximation appears not to have significant deleterious impact on the results, a finding also reported previously by Ricketts et al.[65]

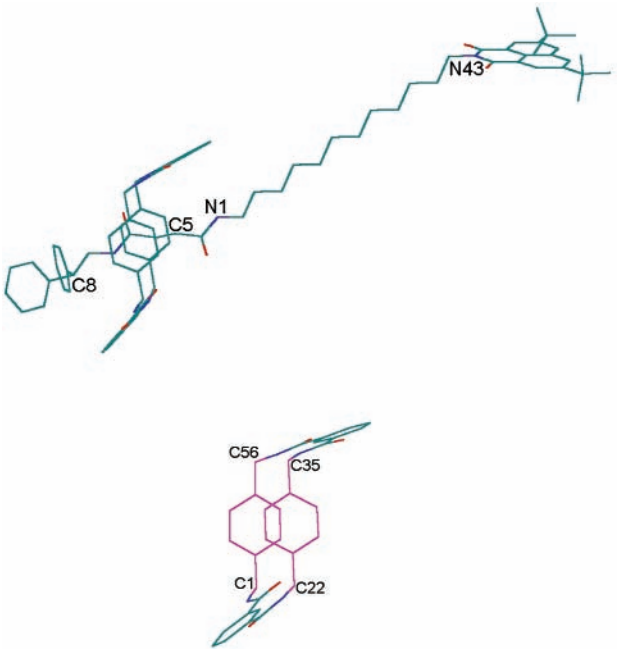

Figure 1. Initial structure of the rotaxane complex. The upper panel shows the complex with the shaft component threaded through the crown component. The atoms labeled C8 and N43 were taken as the left-most and right-most atoms on the shaft component and correspond to the succ and ni stations, respectively. The atoms labeled N1 and N43 were taken to define the line that was used as the axis for the rotation and translation of the crown component. The lower panel shows the crown component only. The atoms within the regions C1−C56 and C22−C35 (except for the H atoms) that are colored in violet were used to define the crown centroid, whose distances to the left-most and right-most atoms (C8 and N43) on the shaft component were used to assign the structure (ni, succ, or middle) of the corresponding coconformations on the basis of the position of the crown component. The three atoms labeled as C1, C22, and C35 were used to define the crown plane.

Structure Generation for Conformational Searching. The initial structure of the rotaxane molecule was generated on the basis of the experimental structure of a closely related system resident in the Cambridge Crystallographic Data Center database[44] [ID CCDC 157381, named (1,4,7,14,17,20-hexaaza-2,6,15,19-tetraoxo-3,5,9,12,16,18,22,25-tetrabenzocyclohexacosane)-(*N*^{1}-{12-[5,8-di(*tert*-butyl)-1,3-dioxo-1*H*-benzo[*de*]isoquinolin-2(3*H*)-yl]dodecyl}-*N*^{4}-(2,2-diphenylethyl)-succinamide)-rotaxane], with the addition of a fully anti-$(CH_2)_{12}$ linear chain spacer between the stoppers. This structure was optimized at the MM level[50−53] to clean the unphysically close contacts. To ensure a thorough conformational searching, the crown component in the initial rotaxane structure was successively rotated around and translated along the shaft component. The rotation was performed with a 36° step size and 360° range. The translation of the crown component for each of these 10 rotations was carried out with a step size of 0.5 Å and a range of 0−8 Å to the left (toward succ) and 0−23 Å to the right (toward ni; see Figure 1). In the initial rotaxane structure, the distances from the center of the crown component to the left end and right end of the shaft component are 7.3 and 22.0 Å, respectively. Here, the C5, C8, and N43 were taken as the center of the crown and the left-most point and the right-most point of the shaft component, successively. The atoms N1 and N43 on the shaft component were taken to define the line that was used as the axis for the rotation and translation of the crown component. In total, 63

TABLE 1: Distances (Å) of the Centroid of the Crown Component to the succ (R_{succ}) and ni (R_{ni}) Sites of the Shaft Component and the Corresponding Structural Assignments

	assignment			
distance	coiled	succ	ni	middle
R_{succ}	<10	<5	>15	otherwise
R_{ni}	<10	>5	<5	otherwise

translations were performed for each of the 10 rotations, generating 630 structures. These 630 structures were then used individually as the starting geometries for the conformational searching. In total, 14 495 coconformations were generated by the conformational searching, covering an energy range of 100 kcal/mol. Of these, 10 118 coconformations were determined to be associated and the other 4377 structures dissociated (i.e., the ring is unthreaded). The dissociated structures were subsequently ignored.

Structural Assignments. To illustrate the relationship of the structural features to energy, single-point calculations were performed at the semiempirical AM1[57] level for all 10 118 associated coconformations, followed by analysis of the correlation between the structural features and energy. In the 10 118 associated coconformations, the shaft component in some conformations is highly folded, while it is extended in others. The ring component prefers to bind at the succ site of the shaft component in some energy ranges while at the ni site in others. Each of the associated structures was, therefore, assigned by its gross structural features (coiled or extended) and by the position of the ring component along the shaft (succ and ni). The distances from the centroid of the crown component to the left-most atom (C8) and the right-most atom (N43) on the shaft component are designated to be R_{succ} and R_{ni}, respectively. C8 in Figure 1 is, therefore, defined as the position of the succ site and N43 as the position of the ni site. Only the atoms highlighted in violet in Figure 1 are chosen to define the centroid of the crown. The centroid defined this way always lies close to the crown plane. The definitions of the structural features (assignments) based on distances R_{succ} and R_{ni} are presented in Table 1. On the basis of visual inspection of a subset of all 10 118 coconformations, it is reasonable to use the cutoff of 10 Å to distinguish the coiled from the extended conformations of the shaft. That is, as shown in Table 1, the structures with both R_{succ} and R_{ni} values less than 10 Å were designated to be coiled; otherwise, they are extended with the ring-component binding at the succ, ni, or middle site.

To further illustrate the distribution of each category of coconformations, the moment-of-inertia tensor **I** and the radius of gyration K (which depends on the largest eigenvalue of the moment-of-inertia tensor and, therefore, reflects to some extent the shape of the corresponding molecule) were computed for the shaft component of each structure and correlated with energy.

Results and Discussion

As demonstrated experimentally,[44] the succ station on one end of the shaft component is an excellent macrocyclic ring-binding site in the ground state. Meanwhile, ni on the other end is a poor H-bond acceptor[66] in the neutral ground state, and the rotaxane adopts the succ coconformation. The H-bond-accepting affinity[66] of ni is greatly enhanced when the shaft is reduced to the anionic state. This reduction may be induced photochemically. It has been observed experimentally that, after photoexcitation by a nanosecond laser pulse, the ni chromophone on the shaft undergoes an intersystem crossing to the triplet state in high yield.[44] A nearby electron donor in solution can induce the formation of a contact-radical ion pair by the reduction of the neutral triplet to the −1 doublet, which enables the shuttling of the macrocyclic ring component down the shaft from its original succ station to the reduced ni unit where ring binding is preferred in the reduced state. A successful modeling procedure should capture this switching behavior, and we will now show how the computations using the procedure described above indeed illustrate this bistability.

Single-Point Calculations and Correlation of the Structural Features to Energy. Figure 2 presents the distribution (number and percentage) of different structural features (extended or coiled) versus energy for the 10 118 associated structures (a and c) and the subset of 116 fully optimized coconformations (b and d) in the neutral singlet state. The number and percentage of extended conformations are predominantly higher than those of coiled conformations, especially in the low-energy regime. As the energy increases, the percent of the extended conformations decreases and the percent of the coiled conformations increases, which shows that the low-energy conformations are predominantly extended rather than coiled for the singlet state. The qualitative distribution is similar for neutral triplet systems (not shown) but has important differences for doublet species, as discussed below.

Further evidence of the energetic preference for extended structures in the singlet state comes from the analysis of the radius of gyration K. Figure 3 presents κ values versus energy for singlet and doublet species on the basis of single-point energy calculations. The κ values are the moving averages of K obtained from all associated coconformations (10 118 total) with an energy width window of 5.0 kcal/mol and a 3.0 kcal/mol overlap. A lower κ value betrays the appearance of some coiled structures. As shown in Figure 3, in the low-energy regime, the doublet species have lower κ values than the singlet species, which indicates that the low-energy structures tend to be more extended in the ground singlet state than in the doublet state. As energy increases, the κ values decrease rapidly for the singlet species while the curve is more flat for the doublet species, so that the κ values of the singlet species become lower than those of the doublet species in the high-energy region.

Preferred Position of the Ring. Figure 4 shows the percentage of succ and ni coconformations versus energy for the singlet (a and b) and doublet (c and d) species. Results based on the single-point energies of the 10 118 coconformations (a and c) and the subset of 116 optimized coconformations (b and d) are displayed. In the low-energy regime, % succ > % ni (a and b) for the singlet species and % ni > % succ (c and d) for the doublet species. Therefore, the low-energy coconformations tend to adopt structures with the crown component binding at the succ station in neutral singlet systems and on the ni station in anionic doublet systems. The situation for the triplet species (not shown) is essentially the same as that for the singlet species.

Figure 5 shows the profile of the system energy versus the position of the ring along the shaft for each of the three electronic states considered. The change in the binding preference with the electronic state is clearly evident. The lowest-energy conformations are located in the 18.0−24.0-Å region for the doublet state (the lowest series), which represents the ni station, while they are in the 3.5−6.5-Å region for the singlet and triplet states, which indicates that the succ coconformations predominate in the latter two states. The energy barrier (ϵ_{act}) for switching to a ni doublet structure from the succ doublet structure, at the value of R_{succ} corresponding to the minimum-energy succ triplet, is ∼11 kcal/mol. From the lowest-energy

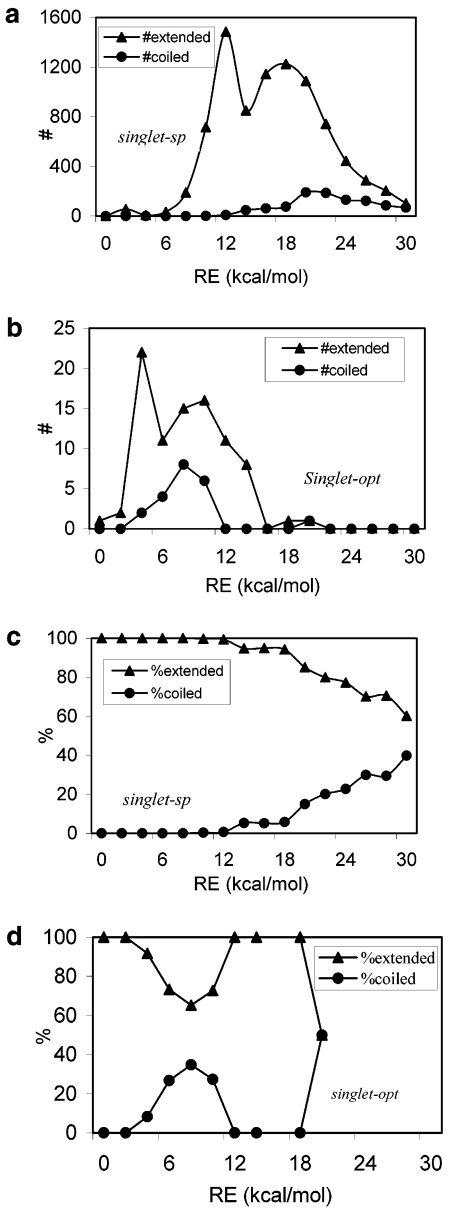

Figure 2. Distribution (number and percentage) versus energy for the coconformations with different backbone (shaft component) structural features (extended or coiled) in the neutral singlet state. Panels a and c are based on single-point calculations for the 10 118 coconformations generated by MM-conformational searching. Panels b and d are for the subset of 116 coconformations fully optimized at the semiempirical level. Note that the single-point calculations and geometry optimizations produce the same qualitative results. For the singlet species, both the number and percentage of the extended coconformations are much higher than those of the coiled coconformations in the low-energy regime. The rotaxane prefers to take on the extended coconformations as its low-energy structure in the singlet state. Energy (RE) is defined relative to the lowest-energy coconformation found for the same state (singlet, doublet, or triplet).

succ doublet structure, ϵ_{act} is ~16 kcal/mol. This should be considered only a crude estimate of the potential-energy barrier to switching. First of all, the curves in Figure 5 represent the energies for selected conformations, not those for a sequence of steps leading from the succ coconformer to the ni coconformer. Second, the AM1 method typically does not provide accurate energy barriers.[61,62] The above caveats notwithstanding, the relatively large barrier, in combination with the significant structural difference between the representative succ singlet and ni doublet coconformers, is consistent with the barrier reported

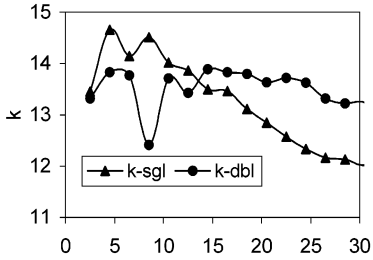

Figure 3. *K*-value distribution versus energy for the singlet and doublet species based on single-point energy calculations, with 5 kcal/mol of width and 3 kcal/mol of overlap for the energy window. The κ values are the moving averages of the radius of gyration *K* for all 10 118 associated coconformations. The *x* axis, which is denoted as RE_{half}, is the middle value of the corresponding energy window. In the low-energy regime, the doublet species (labeled as κ-dbl) have lower κ values than the singlet species.

by Brouwer et al.[44] (10.2 ± 0.7 kcal/mol) and with the observed long time scale for switching (about 1 μs).[44]

Geometry Optimization of a Subset of Conformations. As discussed above, on the basis of the single-point calculations, it may be concluded that the rotaxane strongly prefers coconformations with an extended shaft component at low energy in the singlet and triplet states but displays some coiling tendency in the doublet state. Constructing the profile of structure versus energy in this manner (by using systematic conformational searching followed by semiempirical single-point energy calculations and correlating the structural features to energy) is dramatically less expensive computationally than carrying out full structural optimizations at the semiempirical level for each trial structure. Because a typical geometry optimization requires 500−1000 steps, the use of single-point calculations instead of geometry optimizations decreases the computational expense on the order of 10^3. We propose that, as long as the trial structures generated from the systematic conformational search are "chemically reasonable", the use of single-point calculations will produce a structure-versus-energy profile that is qualitatively consistent with what would be obtained if each structure were fully optimized. (This argument is given with improved theoretical rigor in the Appendix.) To test this proposal numerically, geometrical optimizations were carried out for a subset of coconformations (1 every 100 over the full energy range, totaling 101 coconformations, plus 15 selected low-energy coconformations), including calculations for their ground (singlet), excited (triplet), and anionic (doublet) states. On the basis of experimental results,[44] the triplet state is an intermediate step for the formation of the doublet state from the singlet state. Therefore, the MM-optimized structure was used as the starting geometry for the singlet calculation, while the AM1-optimized singlet geometry was used as the starting geometry for the triplet optimization and the optimized triplet structure was used as the starting geometry for the doublet calculation, consistent with the photoreduction process.

As shown in Figure 2, the single-point and fully optimized calculations recover the same qualitative relationship between the gross structure of the system (coiled or extended) and energy. Figure 4 shows that the same is true for the variation in ring position with energy. Interestingly, while the structure-versus-energy curves produced on the basis of the single-point and fully optimized calculations are qualitatively similar, specific features are skewed to higher energy in the curves based on single-point calculations. This is easily understood on the basis of the error analysis detailed in the Appendix. Because the curves are constructed from calculations (nominally) at minima on the molecular potential-energy surface, any error in deter-

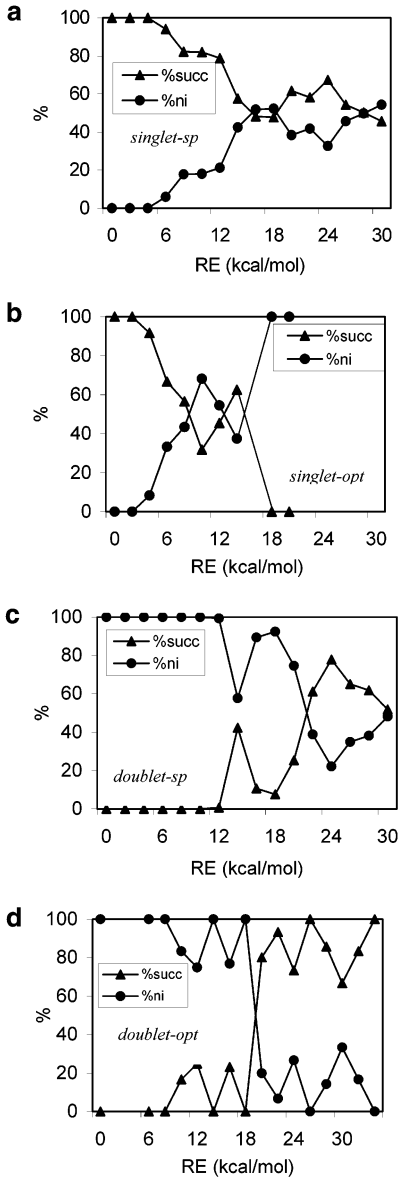

Figure 4. Distribution of conformations versus RE for different assignments of the ring position. Panels a and c are based on 10 118 single-point calculations on the coconformations from MM-conformational searching. Panels b and d are based on 116 coconformations fully optimized at the semiempirical level. Note that the results from the single-point calculations are qualitatively consistent with those from the optimizations. In the singlet state (a and b), % succ ≫ % ni in the low-energy region. The distribution for the doublet state (c and d) is opposite to that for the singlet state, and % ni ≫ % succ for the low-energy coconformations. This indicates that the ring component of rotaxane tends to bind at the succ stations in the singlet species while it prefers the ni station in the doublet state.

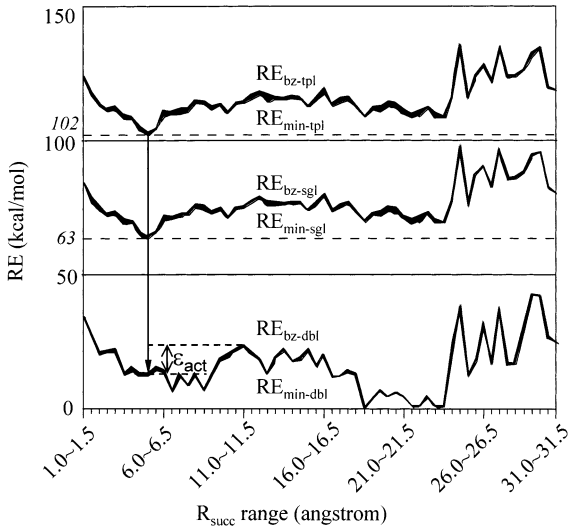

Figure 5. RE-versus-distance (R_{succ}) plots, where RE is the relative energy of the corresponding conformation, which is referenced, for all three states, to the energy of the lowest-energy conformation of the doublet. R_{succ} is the distance of the crown centroid to the succ station of the shaft component as defined in the text. The lower (upper) curves correspond to the lowest-energy points, RE_{min} (Boltzmann average energies, RE_{bz}), in 60 energy windows of 0.5-Å width for each of the three states. Here $RE_{min\text{-}sgl}$ and $RE_{bz\text{-}sgl}$ are for the singlet states, $RE_{min\text{-}dbl}$ and $RE_{bz\text{-}dbl}$ are for the doublet states, and $RE_{min\text{-}tpl}$ and $RE_{bz\text{-}tpl}$ are for the triplet states, respectively. The area between the RE_{min} and RE_{bz} curves is shaded for each state to highlight the difference. $\epsilon_{act} \sim 11$ kcal/mol.

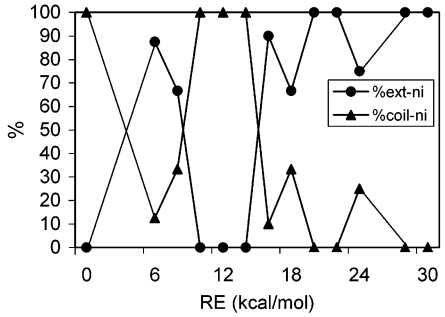

Figure 6. Percentages of extended (% ext-ni) and coiled (% coil-ni) ni structures in the doublet state. RE is the relative energy relative to the lowest doublet-state coconformation. Although the ni coconformations are preferred over the succ coconformation for the doublet species in the low-energy regime as shown in Figure 4 (% ni > % succ), the two types of ni conformations, either extended (ext-ni) or coiled (coil-ni), are competitive with each other, with neither species heavily dominant.

mining the values of the internal coordinates at the minima leads to an energy that is too high. This is because any deviation in the values of the internal coordinates from their values at the true minimum translates into an energy value greater than that at the minimum. This effectively skews features in the energy profile to higher energy. This effect is most clearly evident in Figure 2a,b and may be seen by comparing 2c with 2d, 4a with 4b, or 4c with 4d as well.

For neutral singlet species, as shown in Figure 4, the percentage of coconformations with the ring component binding at the succ station (indicated as % succ) is typically higher than that of the ni coconformations in the low-energy regime. The profile differs for the doublet state, where the ni coconformations dominate in the low-energy regime, with coiled and extended conformations for the shaft component being competitive. Combining the backbone assignments (ext and coil) with the ring-position assignments (succ and ni), we may write "ext-succ", denoting an extended coconformation with the crown component binding at the succ station. Similarly, we may write ext-ni, coil-succ, and coil-ni. The distribution of the extended and coiled coconformations with the ring-component binding at the ni station is presented in Figure 6 for doublet species. ni coconformations exhibit no clear preference for either an extended or a coiled shaft component, suggesting that the extended and coiled structures are competitive.

Ring−Shaft Interaction and Binding Analysis. According to experimental findings,[44] in the ground state the succ station of the shaft component makes an excellent fit with the benzylic macrocyclic ring component, with two sets of bifurcated H

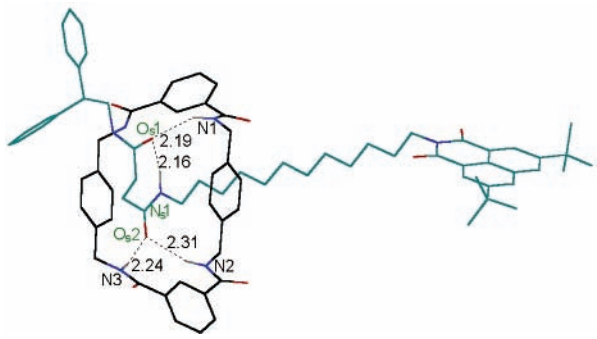

Figure 7. Optimized singlet structure with the lowest energy at the AM1 level. The ring molecule binds at the succ station on the shaft. Hydrogen bonds are marked with dashed lines, with NH···O distances (Å) labeled, and the atoms on the shaft molecule involved in the hydrogen bonds are labeled with a subscript (N_s1, N_s2, etc.). The elements N, O, and H are colored in blue, red, and gray, respectively. The crown component and related atom labels are colored in black, except for the N and O atoms, and the shaft component and related atom labels are colored in green.

bonds formed between the two succ amide carbonyls on the shaft and the isophthalamide groups on the ring. The energy of the rotaxane molecule is, therefore, strongly minimized by the formation of the succ coconformation.[67] The H-binding potential of the ni is greatly increased when it is reduced to a radical anion (doublet species) photo- or electrochemically, which introduces stronger binding with the benzylic amide macrocycle. This enhanced H-binding potential after reduction provides a driving force for the switching of the ring between the original succ and ni stations. These features are accurately captured by our modeling procedure.

The energy order of the three states is typically $E_{\text{doublet}} < E_{\text{singlet}} < E_{\text{triplet}}$. It is reasonable that the triplet has the highest energy among the three states because it is the excited state configuration while the other two are ground-state configurations. The lower energy of the doublet species relative to that of the singlet species indicates a positive gas-phase electron affinity. Representative low-energy coconformations are presented in Figures 7 and 8 for the singlet and doublet species, respectively, with the hydrogen bonds marked as dashed lines together with the corresponding bond lengths. Although the upper limit of a NH···O hydrogen-bond length is reported to be 2.40 Å,[68] the much shorter distances in the coconformations presented here indicate that strong hydrogen bonds are involved in the rotaxane molecule, particularly in light of the fact that the AM1 method tends to slightly overestimate hydrogen-bond lengths.[61]

On the basis of our singlet optimizations, all low-energy structures take on ext-succ coconformations. One such coconformation is shown in Figure 7. The ring component binds at the succ station on the shaft. Two pairs of bifurcated hydrogen bonds are formed between the two component molecules of the rotaxane. The ni unit on the shaft component has no chemical interaction with the ring. The structural preference of the doublet species is different from that of the singlet species. Figure 8 presents three optimized coconformations for the doublet species with lower energy than the other structures. The ring component binds at the ni station on the shaft in all low-energy doublet coconformations. Two pairs of bifurcated hydrogen bonds are formed between the two oxygen atoms (O_s1 and O_s2) on the ni unit of the shaft component and the four amide groups (N1H, N2H, N3H, and N4H) on the ring component, which are denoted as N1H···O_s1, N2H···O_s1, N3H···O_s2, and N4H···O_s2. Additionally, two (panel 8a), one (8b), or zero (8c) additional single

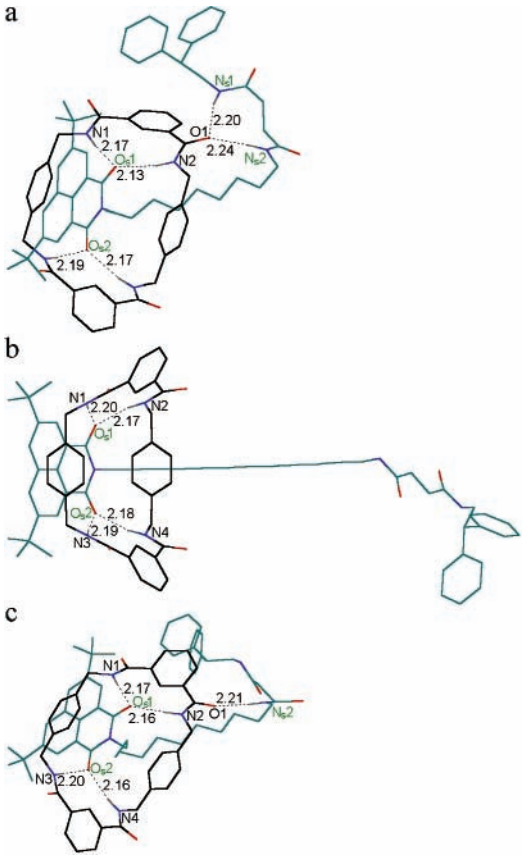

Figure 8. Three coconformations with lower energy than other structures based on doublet optimizations. The ring molecule binds at the ni station on the shaft in all low-energy coconformations. The elements N, O, and H are colored in blue, red, and gray, respectively. The crown component is colored in black, except for the N and O atoms, and the shaft component is colored in green. The hydrogen bonds that are formed between the crown and shaft components are marked with dashed lines, with the corresponding NH···O distances labeled. Two pairs of bifurcated hydrogen bonds are formed between the two oxygen atoms (O_s1 and O_s2) on the ni unit of the shaft and the four amide groups (N1H, N2H, N3H, and N4H) on the ring, which are denoted as N1H···O_s1, N2H···O_s1, N3H···O_s2, and N4H···O_s2, successively. Additionally, two (panel a), one (b), or zero (c) more single hydrogen bonds are involved between the amide groups (Ns1 and/or Ns2) on the succ station of the shaft and the carbonyl group (O1) on the ring component.

hydrogen bonds are involved between the amide groups (N_s1 and/or N_s2) on the succ station of the shaft and the carbonyl group (O1) on the ring component. The shift in structural preference between the singlet and doublet species exhibited in our calculations is in agreement with what was found in experiments,[44] which is that the ring component has the potential to shuttle from the initial succ station to the ni station on the shaft upon photoinduced reduction.

Conclusions

We have carried out a computational study of a rotaxane with photoinduced redox bistability that has been previously demonstrated experimentally.[44] On the basis of calculations of single-point energy and radius of gyration for 10 118 rotaxane structures, succ coconformations predominate in the low-energy regime for the singlet and triplet species, with a preference for the shaft component being extended. The doublet species prefer to take on ni coconformations in low-energy structures, with the coiled and extended conformations being competitive for the shaft component. We obtained effectively the same results

by geometry optimizations of a subset of coconformations. These results are in excellent agreement with previous experimental observations.[44] Therefore, we believe that the structure-versus-energy profile produced in the less-expensive way, by using systematic conformational searching followed by semiempirical single-point energy calculations and correlating the structural features to energy, is consistent with what would be obtained if each structure were fully optimized. We propose that, instead of carrying out full structural optimizations at the semiempirical level for each trial structure, the use of single-point calculations is sufficient to obtain the profile of the structural features versus energy, as long as the trial structures generated from the systematic conformational search are "chemically reasonable".

Acknowledgment. This work was funded in part by the NSF-NER Program, start-up funds from Drexel University, and Dupont Corp. in the form of a Dupont Young Professor award to K.S., who also thanks Prof. K. G. Owens for discussions related to the Appendix.

Appendix

Suppose that we have some function $f(\alpha_i)$, where α_i represents a large number of independent parameters (coordinates) of which there are M. The function is single-valued and continuous and has numerous local minima, indexed n. We assume that in the vicinity of any particular minimum n, the function can be expanded in a quadratic polynomial in the parameters α_i

$$f(\alpha_i^n) \approx c^n + \sum_i [\alpha_i^n - \alpha_i^{\circ n}]^2 \frac{k_i^n}{2} \tag{1}$$

where c^n and k_i^n are constants and $\alpha_i^{\circ n}$ are the values of coordinates α_i at the true minima n. We refer to an expansion about the nth minimum, hence the superscript n. The function $f(\alpha_i)$ describes the potential-energy surface of our rotaxane as a function of its internal coordinates α_i.

We define the function $G(f)$ as the number of minima of $f(\alpha_i)$ with a function value $\leq f$. $G'(f) = \mathrm{d}G(f)/\mathrm{d}f$ is then the density of minima in f, a *density of states* (DOS) function. (This is a density of the conformational states as opposed to the more common density of the electronic states or density of the vibrational states.) $G'(f)$ may be thought of as an energy profile of the system.

Suppose that we have an approximate method of locating the minima n; that is, we can determine the $\alpha_i^{\circ n}$ with finite accuracy and we assume that the errors are randomly distributed. The uncertainty in $\alpha_i^{\circ n}$ translates by propagation of errors into the uncertainty in $f(\alpha_i)$ at the minimum n and ultimately into the uncertainty in $G'(f)$. We seek the influence of error in the prediction of $\alpha_i^{\circ n}$ on the error in the energy profile of the system $G'(f)$. Specifically, if we employ an "approximate" technique (MM) instead of an "exact" one (quantum mechanics) to determine the $\alpha_i^{\circ n}$ and then compute the energies with the exact technique, what effect does this have on the prediction of the energy profile $G'(f)$? Here, the designations "approximate" and "exact" are definitions for the purpose of this derivation. We seek to determine the effect on the energy profile of sampling the structure with one method and computing energies with a different method. Obviously, the AM1 method is an approximate electronic-structure method.

Uncertainty in $f(\alpha_i)$. We will employ the following rules from the standard treatment of propagation of errors:

for a sum $(A \pm \delta A + B \pm \delta B) = C \pm \delta C$

$$\delta C^2 = \delta A^2 + \delta B^2 \tag{2}$$

for a product $(A \pm \delta A)(B \pm \delta B) = D \pm \delta D$

$$(\delta A/A)^2 + (\delta B/B)^2 = (\delta D/D)^2 \tag{3}$$

and for a power $(A \pm \delta A)^t = B \pm \delta B$

$$\delta B/B = t(\delta A/A) \tag{4}$$

Now we present the procedure for determining the $G'(f) \sim f$ relationship.

$$G'(f) = \left.\frac{G(f + \Delta f) - G(f)}{\Delta f}\right|_{\lim \Delta f \to 0} \tag{5}$$

where

$$f(\alpha_i^n) \approx c^n + \sum_i [\alpha_i^n - \alpha_i^{\circ n}]^2 \frac{k_i^n}{2}$$

$$= c^n + \sum_{i=1}^{M} [(\alpha_i^n)^2 - 2\alpha_i^n \alpha_i^{\circ n} + (\alpha_i^{\circ n})^2] \frac{k_i^n}{2} \tag{6}$$

In eq 6, the uncertainties in c^n and k_i^n are zero. If we write $\alpha_i^{\circ n} = \alpha_i^{\circ n} \pm \delta_i^n$, the uncertainties in the three terms inside the sum, $(\alpha_i^n)^2$, $2\alpha_i^n \alpha_i^{\circ n}$, and $(\alpha_i^{\circ n})^2$, are $S_1 = 0$, $S_2 = \pm\delta_i^n$, and $S_3 = \pm 2\alpha_i^{\circ n}\delta_i^n$, respectively. Therefore, the uncertainty in the function $f(\alpha_i)$ is the sum over i ($i = 1-M$) of the uncertainty in $2\alpha_i^n \alpha_i^{\circ n}$, which is $\pm\delta_i^n$, and in $(\alpha_i^{\circ n})^2$, which is $\pm 2\alpha_i^{\circ n}\delta_i^n$. This may be written as

$$\delta f = \sum_{i=1}^{M} [4(\alpha_i^{\circ n})^2(\delta_i^n)^2 + (\delta_i^n)^2]^{1/2} = \sum_{i=1}^{M} \delta_i^n [4(\alpha_i^{\circ n})^2 + 1]^{1/2} \tag{7}$$

according to formula (2). Suppose the maximum value (upper limit) of the uncertainties in α_i^n ($i = 1-M$) is $\pm\delta_i^n$. The operation of the summation in eq 7 then becomes

$$\delta f = \delta_i^n \sqrt{M} [4(\alpha_i^{\circ n})^2 + 1]^{1/2} \tag{8}$$

We may now determine the uncertainty in $G(f)$ and $G'(f)$.

Uncertainty in $G(f)$ and $G'(f)$. The formula

$$\delta G = \delta f\, G'(f)$$

holds as long as $G'(f)$ is slowly varying. Given that

$$G'(f) = \left.\frac{G(f + \Delta f) - G(f)}{\Delta f}\right|_{\lim \Delta f \to 0}$$

the uncertainty in $G'(f)$ is

$$\delta G'(f) = \{[\delta f\, G'(f)]^2 + [\delta f\, G'(f)]^2\}^{1/2} \tag{9}$$

$$\delta G'(f) = \sqrt{2}\, \delta f\, G'(f) \tag{10}$$

It follows that

$$[\delta G'(f)/G'(f)] = \sqrt{2}\, \delta f \tag{11}$$

On the basis of eq 3, where $\delta f = \delta_i^n \sqrt{M}[4(\alpha_i^{\circ n})^2 + 1]^{1/2}$, we may write

$$\delta G'(f) = Q\delta_i^n G'(f) \tag{12}$$

and

$$[\delta G'(f)/G'(f)] = Q\delta_i^n \tag{13}$$

where

$$Q = \sqrt{2}\sqrt{M}[4(\alpha_i^{\circ n})^2 + 1]^{1/2} \tag{14}$$

Therefore, *the relative uncertainty in G′(f) is linearly proportional to the uncertainty in* $\alpha_i^{\circ n}$, the values of the independent parameters at the minima.

We conclude that if values of the $\alpha_i^{\circ n}$ are "chemically reasonable" and as long as $f(\alpha_i^n)$ is computed accurately at these *approximate* minima, the resulting $G'(f)$ will be chemically reasonable as well. Specific to our case, we define the quantum-mechanical (AM1) calculation to be "exact". If the energy $f(\alpha_i^n)$ is calculated exactly (AM1) at the approximate (MM) minima, the error in the resulting DOS will be, at worst, linearly proportional to the errors in the values of the coordinates at the minima $\alpha_i^{\circ n}$. It should be noted that the linear relationship between $\alpha_i^{\circ n}$ and $G'(f)$ is a consequence of the functional form of $f(\alpha_i)$ (see eq 1). This form, however, is equivalent to the harmonic approximation, which enjoys wide application in computational chemistry.[69]

References and Notes

(1) Collin, J. P.; Dietrich-Buchecker, C.; Sauvage, J. P. *Actual. Chim.* **2001**, 27−32.

(2) Collin, J. P.; Gavina, P.; Heitz, V.; Sauvage, J. P. *Eur. J. Inorg. Chem.* **1998**, 1−14.

(3) Amabilino, D. B.; Stoddart, J. F. *Chem. Rev.* **1995**, *95*, 2725−2828.

(4) Pease, A. R.; Jeppesen, J. O.; Stoddart, J. F.; Luo, Y.; Collier, C. P.; Heath, J. R. *Acc. Chem. Res.* **2001**, *34*, 433−444.

(5) Pease, A. R.; Stoddart, J. F. *Mol. Mach. Mot.* **2001**, *99*, 189−236.

(6) Philp, D.; Stoddart, J. F. *Angew. Chem., Int. Ed. Engl.* **1996**, *35*, 1155−1196.

(7) Reuter, C.; Schmieder, R.; Vogtle, F. *Pure Appl. Chem.* **2000**, *72*, 2233−2241.

(8) Chambron, J. C.; Sauvage, J. P.; Mislow, K.; De Cian, A.; Fischer, J. *Chem.—Eur. J.* **2001**, *7*, 4085−4096.

(9) Asakawa, M.; Brancato, G.; Fanti, M.; Leigh, D. A.; Shimizu, T.; Slawin, A. M. Z.; Wong, J. K. Y.; Zerbetto, F.; Zhang, S. W. *J. Am. Chem. Soc.* **2002**, *124*, 2939−2950.

(10) Chiu, S. H.; Rowan, S. J.; Cantrill, S. J.; Ridvan, L.; Ashton, P. R.; Garrell, R. L.; Stoddart, J. F. *Tetrahedron* **2002**, *58*, 807−814.

(11) Biscarini, F.; Cavallini, M.; Leigh, D. A.; Leon, S.; Teat, S. J.; Wong, J. K. Y.; Zerbetto, F. *J. Am. Chem. Soc.* **2002**, *124*, 225−233.

(12) Gunter, M. J.; Bampos, N.; Johnstone, K. D.; Sanders, J. K. M. *New J. Chem.* **2001**, *25*, 166−173.

(13) Hunter, C. A.; Low, C. M. R.; Packer, M. J.; Spey, S. E.; Vinter, J. G.; Vysotsky, M. O.; Zonta, C. *Angew. Chem., Int. Ed.* **2001**, *40*, 2678−2682.

(14) Jeppesen, J. O.; Perkins, J.; Becher, J.; Stoddart, J. F. *Angew. Chem., Int. Ed.* **2001**, *40*, 1216 ff.

(15) Kanamathareddy, S.; Gutsche, C. D. *J. Am. Chem. Soc.* **1993**, *115*, 6572−6579.

(16) Lee, J. W.; Kim, K. P.; Kim, K. *Chem. Commun.* **2001**, 1042−1043.

(17) Osswald, F.; Vogel, E.; Safarowsky, O.; Schwanke, F.; Vogtle, F. *Adv. Synth. Catal.* **2001**, *343*, 303−309.

(18) Schalley, C. A.; Beizai, K.; Vogtle, F. *Acc. Chem. Res.* **2001**, *34*, 465−476.

(19) Leigh, D. A.; Troisi, A.; Zerbetto, F. *Chem.—Eur. J.* **2001**, *7*, 1450−1454.

(20) Li, Z. T. *Chin. J. Org. Chem.* **2000**, *20*, 655−662.

(21) Shukla, R.; Deetz, M. J.; Smith, B. D. *Phys. Chem. Chem. Phys.* **2000**, *2*, 2397−2398.

(22) Jun, S. I.; Lee, J. W.; Sakamoto, S.; Yamaguchi, K.; Kim, K. *Tetrahedron Lett.* **2000**, *41*, 471−475.

(23) Ashton, P. R.; Ballardini, R.; Balzani, V.; Credi, A.; Dress, K. R.; Ishow, E.; Kleverlaan, C. J.; Kocian, O.; Preece, J. A.; Spencer, N.; Stoddart, J. F.; Venturi, M.; Wenger, S. *Chem.—Eur. J.* **2000**, *6*, 3558−3574.

(24) Sohlberg, K.; Sumpter, B. G.; Noid, D. W. *THEOCHEM* **1999**, *491*, 281−286.

(25) Gibson, H. W.; Bryant, W. S. *Abstr. Pap. Am. Chem. Soc.* **1999**, *218*, 102-ORGN.

(26) Amabilino, D. B.; Ashton, P. R.; Balzani, V.; Brown, C. L.; Credi, A.; Frechet, J. M. J.; Leon, J. W.; Raymo, F. M.; Spencer, N.; Stoddart, J. F.; Venturi, M. *J. Am. Chem. Soc.* **1996**, *118*, 12012−12020.

(27) Asakawa, M.; Ashton, P. R.; Iqbal, S.; Quick, A.; Stoddart, J. F.; Tinker, N. D.; White, A. J. P.; Williams, D. J. *Isr. J. Chem.* **1996**, *36*, 329−340.

(28) Anelli, P. L.; Spencer, N.; Stoddart, J. F. *J. Am. Chem. Soc.* **1991**, *113*, 5131−5133.

(29) Ashton, P. R.; Bissell, R. A.; Gorski, R.; Philp, D.; Spencer, N.; Stoddart, J. F.; Tolley, M. S. *Synlett* **1992**, 919−922.

(30) Ashton, P. R.; Bissell, R. A.; Spencer, N.; Stoddart, J. F.; Tolley, M. S. *Synlett* **1992**, 914−918.

(31) Ashton, P. R.; Bissell, R. A.; Spencer, N.; Stoddart, J. F.; Tolley, M. S. *Synlett* **1992**, 923−926.

(32) Ashton, P. R.; Johnston, M. R.; Stoddart, J. F.; Tolley, M. S.; Wheeler, J. W. *J. Chem. Soc., Chem. Commun.* **1992**, 1128−1131.

(33) Ashton, P. R.; Philp, D.; Spencer, N.; Stoddart, J. F. *J. Chem. Soc., Chem. Commun.* **1992**, 1124−1128.

(34) Benniston, A. C.; Harriman, A. *Angew. Chem., Int. Ed. Engl.* **1993**, *32*, 1459−1461.

(35) Bissell, R. A.; Cordova, E.; Kaifer, A. E.; Stoddart, J. F. *Nature (London)* **1994**, *369*, 133−137.

(36) Cantrill, S. J.; Rowan, S. J.; Stoddart, J. F. *Org. Lett.* **1999**, *1*, 1363−1366.

(37) Cao, J. G.; Fyfe, M. C. T.; Stoddart, J. F.; Cousins, G. R. L.; Glink, P. T. *J. Org. Chem.* **2000**, *65*, 1937−1946.

(38) Glink, P. T.; Oliva, A. I.; Stoddart, J. F.; White, A. J. P.; Williams, D. J. *Angew. Chem., Int. Ed.* **2001**, *40*, 1870−1875.

(39) Martinez-Diaz, M. V.; Spencer, N.; Stoddart, J. F. *Angew. Chem., Int. Ed. Engl.* **1997**, *36*, 1904−1907.

(40) Pasini, D.; Raymo, F. M.; Stoddart, J. F. *Gazz. Chim. Ital.* **1995**, *125*, 431−443.

(41) Deetz, M. J.; Shukla, R.; Smith, B. D. *Tetrahedron* **2002**, *58*, 799−805.

(42) Kern, J. M.; Raehm, L.; Sauvage, J. P.; Divisia-Blohorn, B.; Vidal, P. L. *Inorg. Chem.* **2000**, *39*, 1555−1560.

(43) Murakami, H.; Kawabuchi, A.; Kotoo, K.; Kunitake, M.; Nakashima, N. *J. Am. Chem. Soc.* **1997**, *119*, 7605−7606.

(44) Brouwer, A. M.; Frochot, C.; Gatti, F. G.; Leigh, D. A.; Mottier, L.; Paolucci, F.; Roffia, S.; Wurpel, G. W. H. *Science (Washington, D.C.)* **2001**, *291*, 2124−2128.

(45) Wurpel, G. W. H.; Brouwer, A. M.; van Stokkum, I. H. M.; Farran, A.; Leigh, D. A. *J. Am. Chem. Soc.* **2001**, *123*, 11327−11328.

(46) Raymo, F. M.; Houk, K. N.; Stoddart, J. F. *J. Am. Chem. Soc.* **1998**, *120*, 9318−9322.

(47) Leigh, D. A.; Murphy, A.; Smart, J. P.; Deleuze, M. S.; Zerbetto, F. *J. Am. Chem. Soc.* **1998**, *120*, 6458−6467.

(48) Leigh, D. A.; Troisi, A.; Zerbetto, F. *Angew. Chem., Int. Ed.* **2000**, *39*, 350 ff.

(49) Dewart, J.; Zoebisch, E.; Healy, E.; Stewart, J. *HyperchemTM Release 5.01 for WindowsTM*; Hypercube Inc.: Waterloo, Ontario, Canada, 1996; Vol. 107, p 3902.

(50) Dudek, M. J.; Ponder, J. W. *J. Comput. Chem.* **1995**, *16*, 791−816.

(51) Kundrot, C. E.; Ponder, J. W.; Richards, F. M. *J. Comput. Chem.* **1991**, *12*, 402−409.

(52) Ponder, J. W. *Software Tools for Molecular Design*, Version 3.9; 1990−2001 (http://dasher.wustl.edu/tinker/).

(53) Ponder, J. W. *J. Comput. Chem.* **1987**, *8*, 1016−1026.

(54) McDonald, N. A.; Jorgensen, W. L. *J. Phys. Chem. B* **1998**, *102*, 8049−8059.

(55) Jorgensen, W. L.; McDonald, N. A. *THEOCHEM* **1998**, *424*, 145−155.

(56) Jorgensen, W. L.; Maxwell, D. S.; Tirado-Rives, J. *J. Am. Chem. Soc.* **1996**, *118*, 11225−11236.

(57) Dewar, M. J. S.; Zoebisch, E. G.; Healy, E. F.; Stewart, J. J. P. *J. Am. Chem. Soc.* **1985**, *107*, 3902.

(58) Schmidt, M. W.; Baldridge, K. K.; Boatz, J. A.; Elbert, S. T.; Gordon, M. S.; Jensen, J. H.; Koseki, S.; Matsunaga, N.; Nguyen, K. A.; Su, S. J.; Windus, T. L.; Dupuis, M.; Montgomery, J. A. *J. Comput. Chem.* **1993**, *14*, 1347−1363.

(59) Liu, L.; Li, X. S.; Song, K. S.; Guo, Q. X. *THEOCHEM* **2000**, *531*, 127.
(60) Sohlberg, K.; Tarbet, B. J. *J. Inclusion Phenom. Mol. Recognit. Chem.* **1995**, *23*, 203-212.
(61) Buemi, G.; Zuccarello, F.; Raudino, A. *THEOCHEM* **1988**, *164*, 379−389.
(62) Fabian, W. M. F. *J. Comput. Chem.* **1988**, *9*, 369−377.
(63) Dávila, L. Y. A.; Caldas, M. J. *J. Comput. Chem.* **2002**, *23*, 1135−1142.
(64) Levine, I. N. *Quantum Chemistry*; Prentice Hall: Englewood Cliffs, NJ; 1991.
(65) Ricketts, H. G.; Stoddart, J. F.; Hann, M. M. In *Computational Approaches in Supramolecular Chemistry*; Wipff, G., Ed.; Vol. Series C: Mathematical and Physical Science−V426; Kluwer Academic Publishers: Dordrecht, The Netherlands, 1994; pp 377−390.
(66) Niemz, A.; Rotello, V. M. *Acc. Chem. Res.* **1999**, *32*, 44−52.
(67) Fyfe, M. C. T.; Glink, P. T.; Menzer, S.; Stoddart, J. F.; White, A. J. P.; Williams, D. J. *Angew. Chem., Int. Ed. Engl.* **1997**, *36*, 2068−2070.
(68) Vargas, R.; Garza, J.; Friesner, R. A.; Stern, H.; Hay, B. P.; Dixon, D. A. *J. Phys. Chem. A* **2001**, *105*, 4963−4968.
(69) Scott, A. P.; Radom, L. *J. Phys. Chem.* **1996**, *100*, 16502−16513.